2018 5th International Workshop on Compressed Sensing applied to Radar, Multimodal Sensing, and Imaging (CoSeRa)

Sparse Damage Imaging for Guided-Wave Structural Health Monitoring

Christian Vogl, Christian Kexel, and Jochen Moll
Goethe University Frankfurt
Department of Physics
Max-von-Laue-Str. 1
60438 Frankfurt am Main, Germany
Telephone: +49 (0) 69 798-47208
Fax: +49 (0) 69 798-47221
Email: christian.kexel@physik.uni-frankfurt.de

***Abstract*—Guided-wave structural health monitoring is concerned with the detection and localization of defects in thin structures using guided ultrasonic waves which are actuated and sensed by a permanently installed array of piezoelectric transducers. In this work, we analyze sparse recovery algorithms, including Orthogonal Matching Pursuit (OMP), Compressive Sampling Matching Pursuit (CoSaMP), Basis Pursuit De-Noising (BPDN) and Iterative Hard Thresholding (IHT), by studying model-based imaging in a metallic plate possessing a single and multiple damages. A comparison to conventional Delay-and-Sum (DAS) imaging is given based on experimentally obtained data alongside a statistical analysis based on simulations.**

I. Introduction

Regarding signal and image processing there is significant methodological overlap between radar, terahertz applications and systems using guided ultrasonic waves (GUW), because of the similar challenges faced in each of the disciplines. GUW are frequently utilized [1], [2] for evaluating automatically the integrity of structural components, which appear thin compared to the wavelength λ of the GUW. With solely minor dissipation of energy, GUW can travel large distances inside solid structures, including paths across curved walls. Damage assessment using GUW is typically facilitated by a network of transducers which is distributed across the component. In a round-robin manner one actuator excites omnidirectional waves and subsequently sensors acquire the response containing scattering from potential defects. Analysis is then commonly applied to the differential signal, i.e. the residuum between measurements from the intact and damaged structure. Conventionally, less dense networks yield high coverage at the cost of lower spatial resolution. Therefore, a parsimonious ansatz rooted in compressed sensing, is promising in signal recovery scenarios for enhancing localization performance as compared to more classical methods.

In Ref. [3] sparse wavenumber analysis has been employed for reconstructing the multimodal and frequency dispersive properties of GUW propagating in a plate with surface-mounted transducers in order to de-noise signals as well as subtract multipath reflections. In Ref. [4] deconvolution processing has been used for improving the imaging of the sparse acoustic wavefield of an impaired plate which has been scanned using a Laser Doppler Vibrometer. In Ref. [5] a simulation-based dictionary alongside sparse reconstruction, which assumes a structural component to be largely flawless, has been employed for localizing defects in a metallic plate with an array of permanent sensors. This approach has also been studied for potential application in microwave breast cancer detection [6]. Moreover, this approach is deployed and extended in the present work where different sparse recovery algorithms are analyzed for detection and localization in a guided-wave structural health monitoring system.

II. Theoretical Background

A. Lamb Waves

In plate-like solids which exhibit two free boundary surfaces, GUW can be divided into two types. First, the shear-horizontal type shows particle movement vertical to the direction of propagation and parallel to the surfaces. Second, Lamb-type waves show similarly particle movement vertical to the direction of propagation, but furthermore vertical to the surfaces. The frequently encountered scenario in guide-wave monitoring with surface-mounted piezoelectric transducers mostly generates Lamb-type waves.

They exhibit two different variants of wave modes: symmetric and anti-symmetric modes that are labeled S0, S1, ... and A0, A1, ..., respectively. The modes show frequency-dependent wave velocities $v(f)$ and can be interpreted as standing waves across the thickness d of the plate. For any thickness-frequency product $d \cdot f$ distinct symmetric and anti-symmetric modes can emerge. The greater $d \cdot f$, the larger the number of modes. In the present work, the plate has $d = 1.5$ mm and we consider frequencies $f \leq 500$ kHz, therefore only both fundamental modes S0 and A0 can be excited with S0 propagating faster [1].

Numerical simulations of Lamb waves in an isotropic and homogeneous solid, such as an aluminum plate, are carried out by solving the elastodynamic wave equation, taking mass density ρ, Young's modulus E and the Poisson ratio ν (or their equivalents) as parameters.

B. Problem Formulation

Generally, we consider a pre-recorded time-domain baseline signal $\underline{y}^{\text{base}}(t)$ from the pristine structures without defects. For defect detection the difference signal $\underline{y}^{\text{diff}}(t)$ is calculated containing both information about scatterers and an additional noise term:

$$\underline{y}^{\text{diff}}(t) = \underline{y}^{\text{measured}}(t) - \underline{y}^{\text{base}}(t) = \underline{y}^{\text{scattered}}(t) + \underline{e}(t) \quad (1)$$

The γ-th signal $\underline{y}_{\gamma}^{\text{measured}}$ is obtained by a pitch-catch measurement between a pair of transducers. A total number of P signals is acquired. Each signal possesses L samples.

In a linear formulation of the problem

$$\underline{y}_{\gamma}^{\text{diff}} = \underline{\underline{A}}_{\gamma} \cdot \underline{x} + \underline{e}_{\gamma} \quad (2)$$

the differential signal is assumed to contain a linear superposition of scattering effects by localized damages. The monitored area is represented by $\underline{x} \in \mathbf{R}^M$ where each non-zero entry x_m should represent a defect in the plate at pixel $m \in \{1, M\}$ and $\underline{\underline{A}}_{\gamma}$ is the dictionary of transducer pair γ. Thus $a_{\gamma,m}$ is the m-th column of $\underline{\underline{A}}_{\gamma}$, corresponding to the expected difference signal of a defect located at pixel m. This expected difference signal and thus the dictionary is generated by numerical simulation of GUW. The dictionary is a collection of simulated signals stemming from a scatterer at every possible point in the discretized plate.

If we treat all transducer pairs, we get a system of equations:

$$\begin{aligned} \underline{y}_1^{\text{diff}} &= \underline{\underline{A}}_1 \cdot \underline{x} + \underline{e}_1 \\ \underline{y}_2^{\text{diff}} &= \underline{\underline{A}}_2 \cdot \underline{x} + \underline{e}_2 \\ &\vdots \\ \underline{y}_P^{\text{diff}} &= \underline{\underline{A}}_P \cdot \underline{x} + \underline{e}_P \end{aligned} \quad (3)$$

Since $\underline{x}$ is the same in all equations, we can finally concatenating all $\underline{y}_{\gamma}^{\text{diff}}$ yielding $\underline{y}^{\text{diff}} \in \mathbf{R}^{L \cdot P}$ and all dictionaries yielding $\underline{\underline{A}} \in \mathbf{R}^{L \cdot P \times M}$.

C. Recovery Algorithms

So as to approximate solutions, we employ different sparse recovery algorithms which we briefly review, for details however the reader is referred to the original publications.

1) OMP: It casts the problem into the minimization:

$$\min_x ||\underline{y} - \underline{\underline{A}} \cdot \underline{x}||_2 \qquad \text{with} \quad ||\underline{x}||_0 \leq S \quad (4)$$

where S denotes a given sparsity of the solution, the number of non-zero entries in $\underline{x}$ and where $||...||_0$ denotes the zero norm. This greedy algorithm attempts to find the pixel which minimizes the residual in each of the S iterations [7].

2) CoSaMP: It is similar to OMP, but possesses theoretical performance guarantees [8]. Mathematically the solution is cast as the optimization problem:

$$||\underline{x} - \underline{a}||_2 \leq C \cdot \max_x \left\{ \eta, \frac{1}{\sqrt{S}} ||\underline{x} - \underline{x}_{\frac{S}{2}}||_1 + ||\underline{e}||_2 \right\} \quad (5)$$

where C denotes a constant bound, $\underline{a}$ is the computed signal approximation, η is the given precision and $\underline{x}_{\frac{S}{2}}$ is the best $\frac{S}{2}$ sparse approximation of $\underline{x}$.

3) BPDN: It performs a convex optimization [9]:

$$\min_x \frac{1}{2} ||\underline{y} - \underline{\underline{A}} \cdot \underline{x}||_2 + \mu ||\underline{x}||_1 \quad (6)$$

where μ is a regularization parameter.

4) IHT: It belongs to the class of iterative algorithms with thus low computational complexity and small memory requirements. In iteration k IHT approximates the signal $\underline{x}$ as $\underline{x}^k$ [10]:

$$||\underline{x} - \underline{x}^k||_2 \leq 2^{-k} ||\underline{x}^S||_2 + 5\epsilon_S \quad (7)$$

where

$$\epsilon_S = ||\underline{x} - \underline{x}^S||_2 + \frac{1}{\sqrt{S}} ||\underline{x} - \underline{x}^S||_1 + ||\underline{e}||_2 \quad (8)$$

IHT does this by successively applying the formula:

$$\underline{x}^{[n+1]} = H_s \left(\underline{x}^{[n]} + \underline{\underline{A}}^T \cdot (\underline{y} - \underline{\underline{A}} \cdot \underline{x}^{[n]}) \right) \quad (9)$$

where the thresholding operator H_s sets all but the s-highest entries to zero. It is known that IHT can suffer from slow convergence [11].

5) Conventional Imaging: We compare the sparse recovery algorithms against classical DAS imaging which is also used in radar systems to perform synthetic focussing [12]. Here, for each pixel m the time-domain signal of each of the P actuator-sensor-combinations is delayed by τ according to the length $D = D_A + D_S$ of the path from actuator to pixel D_A and the path from m to the sensor D_S. Hence, the wave's group velocity v is required. The delayed signals are uniformly superimposed in order to build up a spatial intensity distribution where high intensities correspond to potential scatterers [13].

III. Setup and Pre-Processing

In general, for the simulation studies and the experiment, the same arrangement is considered: a thin aluminum plate with dimensions 500 x 500 x 1.5 mm and twelve piezoelectric surface-mounted transducers which are placed near the edges of the plate with six on each of the opposite sides of the same surface. The exact positions are shown in Fig. 1. For the measurement a multichannel device [14] records the pitch-catch signals in round-robin turns.

Measured signals are smoothed using a median filter of window width 3. For further processing, we extract only the first wave packet of the multimodal signal. This is accomplished by detecting the onset of the packet using a significant increase in the signal's envelope.

IV. Results

A. Single-defect Imaging

First, we study experimentally a plate with one through-hole. For construction of the simulation-based dictionary, its area is partitioned into 40 x 40 pixels. The results employing GUW with $f = 200$kHz are displayed in Fig. 1.

For OMP, sparsity must be chosen a priori: we set $S = 10$ which is higher than the number of defects expected inside a previously pristine component. So as to omit unreasonable

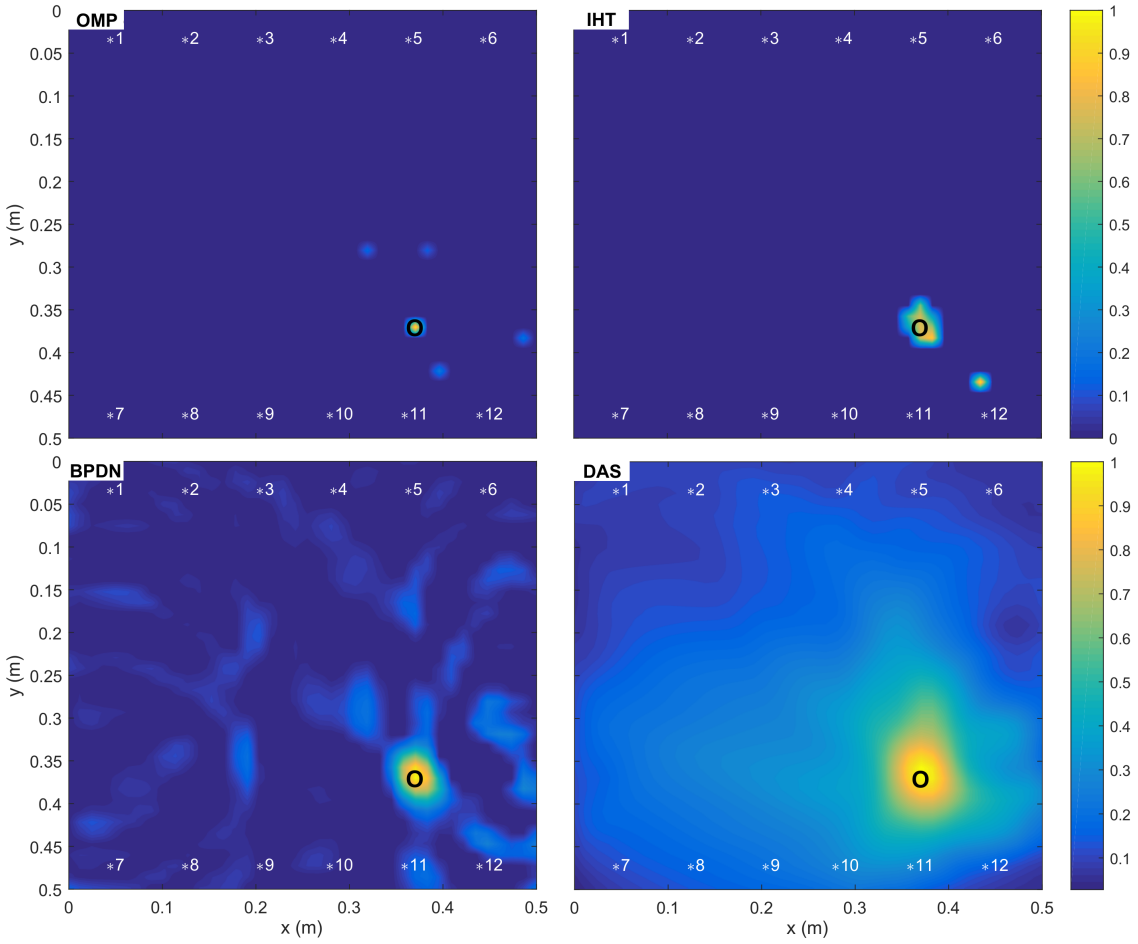

Fig. 1. Comparison of OMP, IHT, BPDN and DAS (from left to right, top to bottom). True position of the defect is marked by the circle. Transducer positions are labeled by number. Intensities are normalized to lie in the interval between 0 and 1.

solutions, negative entries are removed from the solution vector. OMP successfully localizes the damage with sharp resolution (1 pixel), but some spurious spots (with smaller amplitude) close to the actual scatterer emerge. The spots appear because of the over-estimated level of sparsity. They vanish for reconstruction using $S = 1$. CoSaMP has not been included as a separate plot, because it yields results equivalent to OMP, but at slower run time.

Also for IHT entries below zero are zeroized in the solution vector. IHT is run for 30 iterations. In Fig. 1 IHT leads to a clear localization of the damage and one pronounced side peak. We have found that the more iterations used, the better are the results regarding falsely detected defects.

BPDN is also run for 30 iterations, values less than zero solution-entries are removed. BPDN yields a maximum at the damage's location, however also clutter in the remaining area.

The non-sparse approach DAS leads to a continuous intensity distribution with a correct maximum at the through-hole position.

B. Multiple-defects Imaging

Then we investigate experimentally a plate with three through-holes, but other parameters remain unchanged. Results are given in Fig. 2.

Again CoSaMP leads to similar results like OMP. OMP/CoSaMP sharply reconstructs two defects. A recovered peak lies close to the actual third damage, but due to its reduced intensity it is hard to discriminate between true defect and spurious spots.

IHT finds the three defects, but also generates further peaks with about the same amplitude. The size of the found damages is not as sparse as the OMP/CoSaMP results. This can be caused by the small number of 30 iterations.

BPDN reconstructs the holes, but the reconstructed intensity is blurred making it impossible to identify the number of defects. Again, clutter is present in the whole monitored area.

With DAS one cannot distinguish between all three points because the maxima overlap significantly, however strong intensity is correctly assigned to the actual position of the three damages.

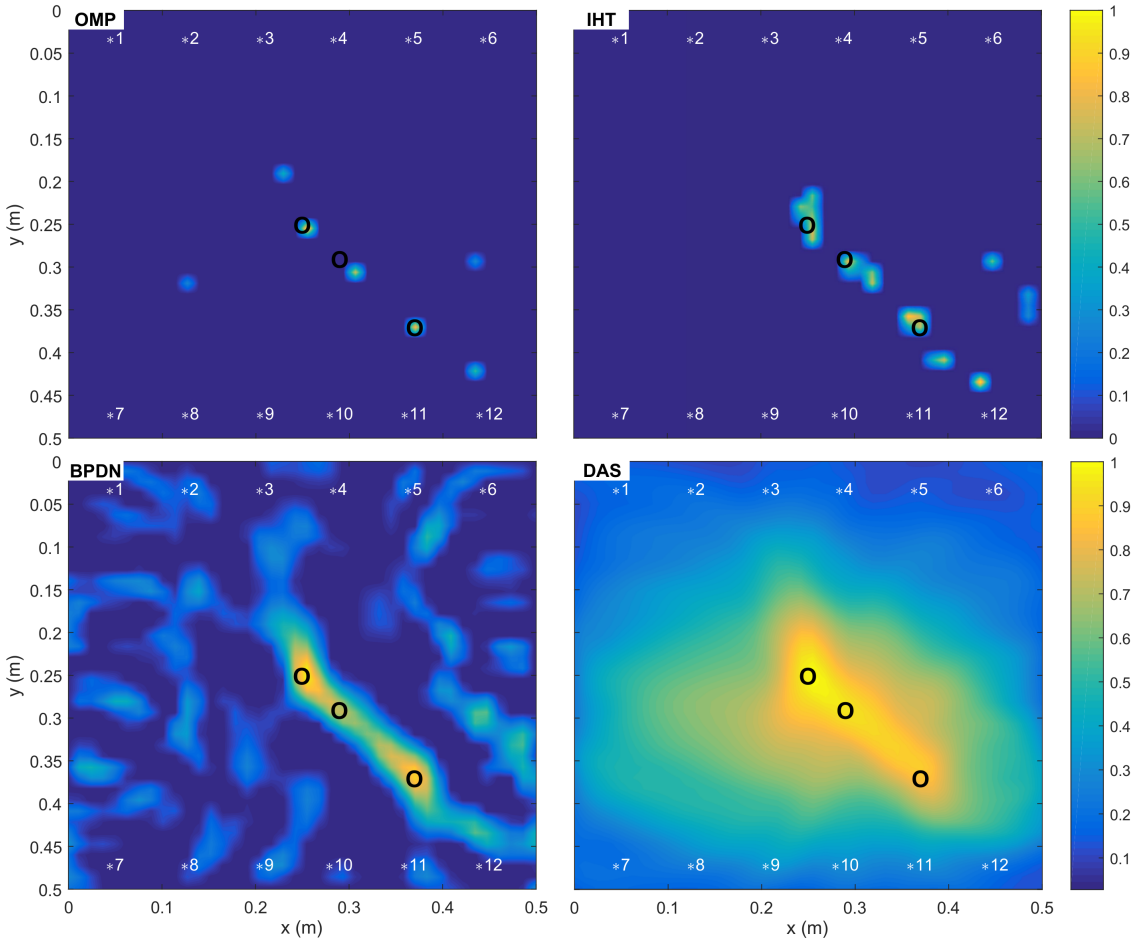

Fig. 2. Comparison of OMP, IHT, BPDN and DAS (from left to right, top to bottom). True positions of the defects are marked by circles.

C. Statistical Study of Single-defect Intensity Recovery

In order to further analyze the sparse recovery algorithms, we conduct numerical simulations where the intensity, i.e. reflectivity, is varied. On 26 x 26 pixels grid, we place one artificial scatterer and repeat the reconstruction procedure 200 times with different random amplitudes drawn from a uniform distribution. Such a simulation set is performed for different levels of noise where the signals are contaminated with normally distributed noise having zero mean and a standard deviation of

$$\sigma \cdot \max_t \left(\underline{y}^{\text{diff}}(t)\right) \tag{10}$$

where the noise level is denoted by σ and is given relative to the maximal of the differential signal. Again, $f = 200$kHz.

In Fig. 3 the histograms of the relative recovered intensities at the scatterer's pixel is presented. Perfect reconstruction corresponds to a single bin with relative frequency of 1 at a value of 1 on the x-axis. The more the actual distribution is shifted away from that ideal distribution, the worse we consider the algorithm's performance. We specifically compare the statistical mean of each distribution.

Results for OMP and CoSaMP are nearly the same. We present here the CoSaMP plot. At noise levels 0 and 0.1, CoSaMP/OMP and BPDN exhibit roughly the same mean of the respective distribution with IHT having a clearly lower mean value. At noise levels 0.5 and 1.0, CoSaMP/OMP outperform both other algorithms with IHT being superior to BPDN in this regard. However, in comparison to the other algorithms IHT has the highest percentage of non-reconstructed cases (meaning zero relative reconstructed intensity).

D. Analysis of Double-defect Intensity Recovery

Finally, we explore the ability of OMP to reconstruct two flaws quantitatively. Here, a smaller plate with dimensions 250 x 250 x 1.5mm is considered. The first damage is fixed at its center. For the second damage all other pixel positions out of the 40 x 40 pixels are probed. We calculate the fraction of damages that could be reconstructed as a function of radial distance from the central flaw. At distances below 2cm, due to the imposed discretization of the plate, not enough data points were simulated to create a meaningful average. These small distances are left out in Fig. 4.

With increasing frequency f the higher the fraction of points that can be reconstructed at short between-defect distances. This can be explained by the decreasing wavelength $\lambda = v(f)/f$ and hence increased resolution.

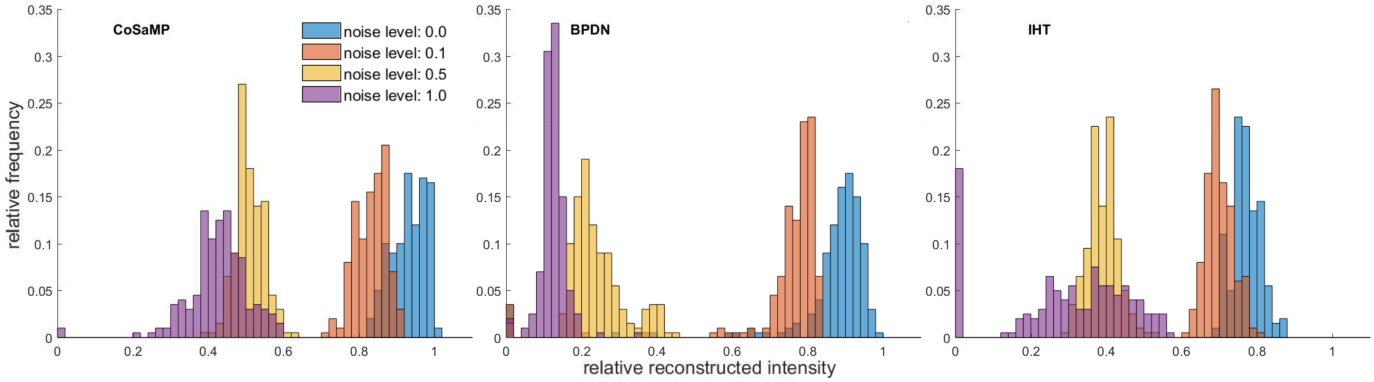

Fig. 3. Comparison of CoSaMP, BPDN and IHT (from left to right). The definition of noise levels is discussed in the text.

V. Conclusions and Outlook

We have studied popular sparse recovery algorithms for model-based damage imaging in a plate structure comprising a single as well as multiple damages. Orthogonal Matching Pursuit (OMP) as well as Compressive Sampling Pursuit (CoSaMP) deliver equivalent results and localization of the single defect with a resolution of 1 pixel and minor clutter. For a scenario with three through-holes OMP/CoSaMP and Iterative Hard Thresholding (IHT) yield the best results with clear discrimination of individual scatters, although none of the algorithms allow for the exact determination of the number of the point-like flaws. Moreover, regarding the reconstruction of defect intensities OMP/CoSaMP perform best on noise contaminated signals. OMP is furthermore in our comparison the algorithm with the fastest run time. However, we considered IHT in its original variant, disregarding subsequent improvements in speed [11].

VI. Acknowledgements

The authors are grateful to Klaus Neuschwander for providing the measurement data. The authors acknowledge the support by the German Research Foundation (grant 349435502) and the Federal Ministry for Economic Affairs and Energy (grant 03SX422B).

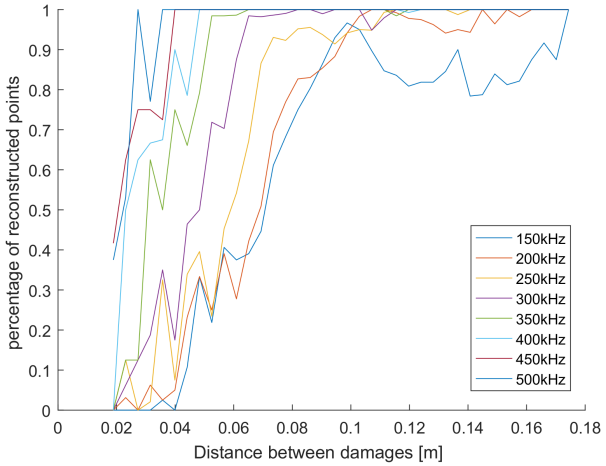

Fig. 4. Frequency-dependent ability of OMP to recover two separated defects.

References

[1] V. Giurgiutiu, *Structural health monitoring: with piezoelectric wafer active sensors*. Academic Press, 2014.

[2] M. Mitra and S. Gopalakrishnan, "Guided wave based structural health monitoring: A review," *Smart Materials and Structures*, vol. 25, p. 053001, May 2016.

[3] J. B. Harley and J. M. Moura, "Sparse recovery of the multimodal and dispersive characteristics of lamb waves," *The Journal of the Acoustical Society of America*, vol. 133, no. 5, pp. 2732–2745, 2013.

[4] C. Kexel and J. Moll, "Deconvolution Processing for Improved Acoustic Wavefield Imaging," *Case Studies in Nondestructive Testing and Evaluation*, vol. 2, pp. 77–83, 2014.

[5] R. M. Levine and J. E. Michaels, "Model-based imaging of damage with lamb waves via sparse reconstruction," *The Journal of the Acoustical Society of America*, vol. 133, no. 3, pp. 1525–1534, 2013.

[6] C. Kexel, J. Moll, M. Kuhnt, F. Wiegandt, and V. Krozer, "Compressed Sensing for Three-Dimensional Microwave Breast Cancer Imaging," in *8th European Conference on Antennas and Propagation*, pp. 1634–1638, 2014.

[7] Y. C. Pati, R. Rezaiifar, Y. C. P. R. Rezaiifar, and P. S. Krishnaprasad, "Orthogonal matching pursuit: Recursive function approximation with applications to wavelet decomposition," in *Proceedings of the 27 th Annual Asilomar Conference on Signals, Systems, and Computers*, pp. 40–44, 1993.

[8] D. Needell and J. Tropp, "Cosamp: Iterative signal recovery from incomplete and inaccurate samples," *Applied and Computational Harmonic Analysis*, vol. 26, no. 3, pp. 301 – 321, 2009.

[9] E. van den Berg and M. P. Friedlander, "Probing the pareto frontier for basis pursuit solutions," *SIAM Journal on Scientific Computing*, vol. 31, no. 2, pp. 890–912, 2008.

[10] T. Blumensath and M. E. Davies, "Iterative hard thresholding for compressed sensing," *Applied and Computational Harmonic Analysis*, vol. 27, no. 3, pp. 265 – 274, 2009.

[11] T. Blumensath, "Accelerated iterative hard thresholding," *Signal Processing*, vol. 92, no. 3, pp. 752–756, 2012.

[12] J. Moll, C. Kexel, and V. Krozer, "A Comparison of Beamforming Methods for Microwave Breast Cancer Detection in Homogeneous and Heterogeneous Tissue," in *10th European Radar Conference (EuRAD)*, (Nuremberg, Germany), pp. 527–530, 2013.

[13] J. Moll, L. De Marchi, C. Kexel, and A. Marzani, "High resolution defect imaging in guided waves inspections by dispersion compensation and nonlinear data fusion," *Acta Acustica united with Acustica*, vol. 103, no. 6, pp. 941–949, 2017.

[14] K. Neuschwander, A. Shreshta, J. Moll, V. Krozer, and M. Bücker, "Multichannel device for integrated pitch catch and emi measurements in guided wave structural health monitoring applications," in *11th International Workshop on Structural Health Monitoring*, 2017.